Thermally tunable Silicon polarization rotator based on mode hybridization

(Student paper)

Theoni Prousalidi[1,2], Giannis Poulopoulos[1], Carmelo Scarcella[2], Harry Zervos[1], Daisy Bergin[2,3], Anthony Bulling[2], Stéphane Detraz[2], Milana Lalović[2,4], Leonardo Marcon[2], Lauri Olanterä[2], Ulrik Sandven[2], Christophe Sigaud[2], Csaba Soos[2], Jan Troska[2] and Hercules Avramopoulos[1]

[1]School of Electrical and Computer Engineering, National Technical University of Athens, 15780 Zografou, Athens, Greece
[2] CERN, Esplanade des Particules 1, 1211 Geneva, Switzerland
[3] University of Bath, Claverton Down, Bath BA2 7AY, UK
[4] School of Electrical Engineering, University of Belgrade, Belgrade, Serbia
[*] theoni.prousalidi@cern.ch

A novel thermally tunable polarization rotator based on mode hybridization, is presented. The proposed component features a compact device footprint of 15.5 µm, insertion loss of 2.25 dB, and PER value above 13 dB across the entire C-band. By exploiting a thermal tuning mechanism, PER higher than 30.5 dB over 15 nm range is achieved with 3.5 mW/nm tuning efficiency.
Keywords: *Silicon Photonics, polarization rotator, thermal tuning, mode hybridization*

INTRODUCTION

Silicon Photonics platform (SiPh) is playing an important role in optical communications due to its compatibility with complementary metal oxide semiconductor (CMOS) fabrication processes [1] and the availability of multi-project wafer (MPW) services [2], while enabling highly integrated circuits with compact footprint and low power consumption. However, the high index contrast of SiPh induces strong birefringence and, thus, polarization dependent waveguiding. On-chip polarization diversity circuits can be exploited to overcome the polarization dependence [3]. In addition, they enable polarization division multiplexing (PDM) schemes that can be used to double link capacity [4]. A key component to enable on-chip polarization diversity is the polarization rotator (PR). PRs can be based on different techniques, such as mode coupling, mode evolution [5],[6] and mode hybridization [7], while other more advanced configurations, such as plasmonic [8] or subwavelength structures [9], can achieve increased performance. However, such solutions suffer from high insertion loss and low polarization extinction ratio (PER), or require complex integration and fabrication processes, respectively.

In this work, we propose a thermally tunable polarization rotator, based on mode hybridization, which features a compact device length of 15.5 µm with insertion loss of 2.25 dB and PER > 13 dB across the C-band. By exploiting the thermal tuning mechanism, PER higher than 30.5 dB over 15 nm range is achieved with 3.5 mW/nm tuning efficiency. The tuning mechanism presented requires low power and enables the integration of a high PER polarization rotator component in flex-grid DWDM systems, and in circuits with varying temperature operational requirements. The component is compatible with MPW services and is highly tolerant against fabrication variations.

SIMULATIONS AND DESIGN

The polarization rotator consists of an intermediate rotator segment, shaped as a single-stair waveguide, connecting an input and an output wire waveguide (Figure 1 (a)). By breaking the symmetry of the waveguide cross-section, the supported propagation modes are hybridized, whereas by changing the rotator segment length (*L*) the state of the polarization at the output waveguide can be selected. The rotator segment supports two hybrid modes (Figure 1 (b),(c)) with their optical axes perpendicular to each other. The optical axis is calculated in Eq.(1) [10]:

$$tan\,\theta = \frac{\iint_{\Omega} n^2(x,y)\cdot H_x^2(x,y)dxdy}{\iint_{\Omega} n^2(x,y)\cdot H_y^2(x,y)dxdy} \quad (1)$$

where $n(x,y)$ is the refractive index distribution profile, while $H_x(x,y)$ and $H_y(x,y)$ are the x- and y- components, respectively, of the magnetic field of the hybrid mode.

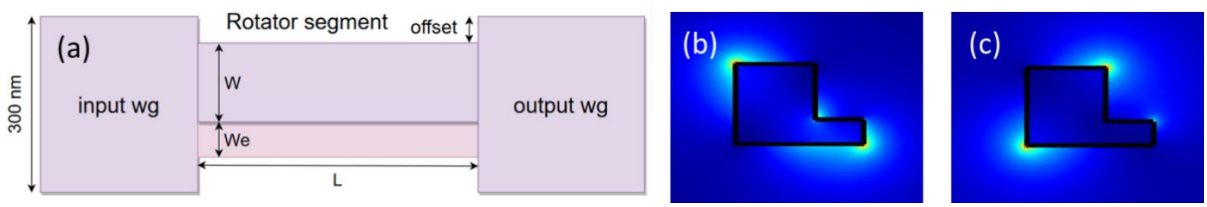

Figure 1: (a) Top View of the geometry of the proposed polarization rotator, (b) first hybrid mode, and (c) second hybrid mode.

Since the hybrid modes have different effective refractive indices and therefore different propagation constants (β_1 and β_2), while they propagate in the rotator segment they accumulate a phase difference. For π rad phase difference polarization rotation is achieved. This condition is fulfilled for rotator segment length equal to the conversion length, given by Eq. (2):

$$L_\pi = \frac{\pi}{\beta_1 - \beta_2} \tag{2}$$

The rotator segment can be characterized by the polarization conversion efficiency (PCE), given by Eq. (3) in [10]:

$$PCE = 4\,sin^2\,\theta\,cos^2\,\theta\,sin^2\left(\frac{\pi L}{2L_\pi}\right) \times 100\% \tag{3}$$

where θ is the optical axis of the first hybrid mode, L_π is the conversion length and L the actual length of the rotator segment. To achieve maximum PCE three requirements must be met. Firstly, the hybrid modes should be equally TE and TM polarized, thus their optical axes need to be near 45°. Secondly, both hybrid modes are targeted to be equally excited by the input modes and finally the actual length L of the segment must be equal to L_π. Considering these, simulations were performed to determine the optimal geometrical parameters of the rotator segment. A topview of the rotator is shown Figure 1(a) which was simulated in the 220 nm SOI with 3 µm BOX integration platform. The rotator segment single step is formed via etching part of the waveguide as shown in Figure 1(a), where W is the width of the unetched part, and W_e the width of the etched part of the waveguide (150 nm etch depth). Finite Difference Eigenmode (FDE) simulations varying a set of (W, W_e) pairs were performed, to optimize the intermediate segment rotation efficiency. Calculated hybrid mode profiles are shown in Figures 1(b) and (c). In Figure 2, the calculated results regarding theta (θ) angle and PCE, are plotted varying (W, W_e) pair values. The set of pairs for which the optical axis is close to 45° and the PCE near 100% is shown in dark red in the PCE plot (Figure 2(b)).

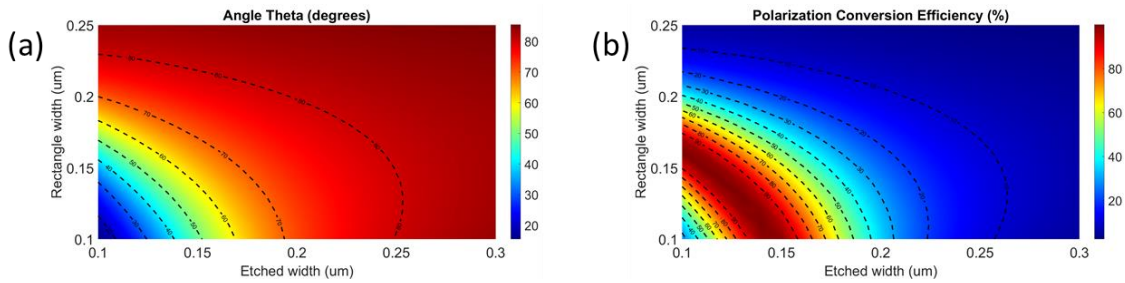

Figure 2: Calculated (a) angle theta and (b) PCE values of the rotator segment, for L = L_π, varying (W, We) pairs.

To calculate the overall component's efficiency, a set of EigenMode Expansion (EME) propagation simulations are carried out considering the rotator segment and input/output waveguides. In these simulations, input/output waveguides width value as well as the lateral offset between them and the intermediate segment (Figure 1(a)), are optimized to achieve equal excitation of the two hybrid modes, and minimise the interface insertion losses. Having defined the optimum lateral offset and input/output waveguides width (300 nm - 450 nm), for each pair of (W, W_e) values, the TE efficiency (TM mode excited at input) and Polarization Extinction Ratio (PER) values are presented in Figure 3(a), and (b), respectively, calculated via 3D-EME simulations.

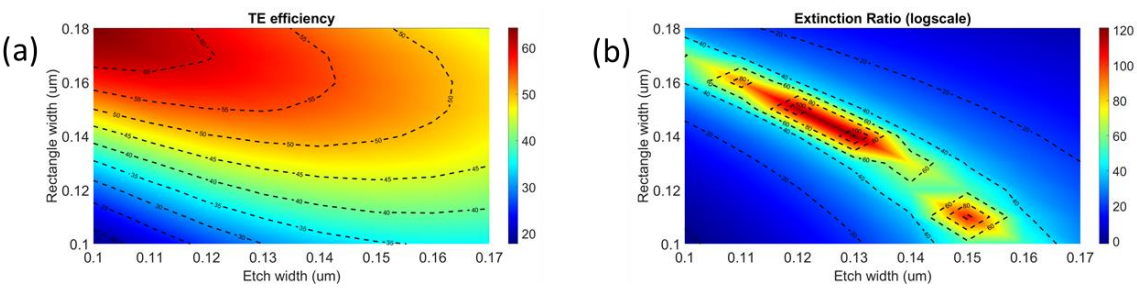

Figure 3: Calculated (a) TE efficiency and (b) PER at rotator output varying (W, We) values, for optimized lateral offset and L=L_π.

W and W_e values that result in maximum TE efficiency, and the corresponding values of lateral offset, can be identified. Optimum geometrical characteristics can be found with dark red in these plots (Figure (3)), while the final design parameters deduced are W=170 nm, W_e=100 nm, and *lateral offset*=-60 nm. A tolerance study was then carried out, investigating the effect of ±10% variation in the etch depth and waveguide height, around 150 nm and 220 nm, respectively. TE efficiency remains above 53% for up to ±15 nm etch depth variation (Figure 4 (a)), and 50% for up to ±10 nm silicon waveguide height variation (Figure 4 (b)), showcasing relaxed fabrication requirements of the component and full compatibility with fabrication in Silicon Photonics MPW services.

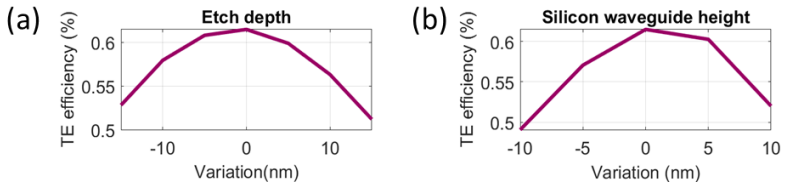

Figure 4: Rotator efficiency versus (a) etch depth variation and (b) Si waveguide height variation for $L=L_{\pi}$.

The spectral performance of the rotator, calculated with 3D-EME and validated with 3D-FDTD simulations, is shown in Figure 5(a). TE efficiency, TM efficiency and PER value (right axis), reveal broadband operation centred around 1550 nm, where 62% TE efficiency and 30.5 dB PER is achieved. Over the entire C-band, TE efficiency > 59.5% and PER > 13 dB is achieved.

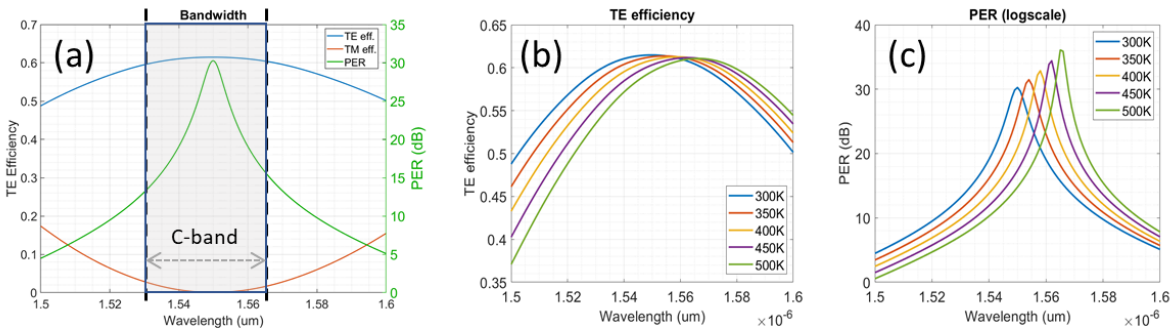

Figure 5: (a) Proposed rotator spectral performance. (b) TE efficiency and (c) PER values for different temperatures.

Thermal tuning of the component is achieved through a 1.5 µm wide metal heater wire placed 1 µm above the rotator segment waveguide. By applying DC voltage, the rotator segment temperature can be adjusted thusly tuning the refractive index exploiting the thermo-optic effect. The thermo-optic coefficients used for Si and SiO_2 were 1.8×10^{-4} and 1×10^{-5} respectively, with reference temperature of 300 K. EME simulation results for TE efficiency and PER values, varying temperature from 27 °C to 227 °C (300 K to 500 K) are shown in Figure 5(b) and (c), respectively. A 0.075 nm/°C central wavelength redshift is calculated for both TE efficiency and PER values, resulting in a 3.5 mW/nm power tuning efficiency. This low-power thermal tuning mechanism allows this polarization rotator to be used in applications under changing temperature environments where thermal tuning is necessary to ensure maximum PER in a specific wavelength. In addition, it can be deployed as a key element in elastic optical networks where wavelength tunability and high PER are indispensable requirements.

CONCLUSIONS

We presented a novel broadband polarization rotator element designed for 220-nm top SOI integration platform. It is characterized by a short length of 15.5 µm, insertion loss of 2.25 dB and PER value above 13 dB across the entire C-band. By exploiting the thermal tuning mechanism, PER value higher than 30.5 dB over 15 nm range is achieved with 3.5 mW/nm tuning efficiency. Its low fabrication complexity and low power consumption enable its adoption across many polarization diversity photonic integrated circuits and elastic optical network deployments.

ACKNOWLEDGMENTS

This work was supported by the European Commission, through H2020-QAMELEON project (780354).

References

[1] W. Bogaerts and L. Chrostowski, “Silicon photonics circuit design: methods, tools and challenges,” *Laser \& Photonics Rev.*, vol. 12, no. 4, p. 1700237, 2018.
[2] M. Pantouvaki *et al.*, “50Gb/s silicon photonics platform for short-reach optical interconnects,” in *Optical Fiber Communication Conference*, 2016, pp. Th4H--4.
[3] H. Fukuda et al., “Silicon photonic circuit with polarization diversity,” *Opt. Express*, vol. 16, no. 7, pp. 4872–4880, 2008.
[4] C. Li, D. Liu, and D. Dai, “Multimode silicon photonics,” *Nanophotonics*, vol. 8, no. 2, pp. 227–247, 2019.
[5] Y. Yin, Z. Li, and D. Dai, “Ultra-broadband polarization splitter-rotator based on the mode evolution in a dual-core adiabatic taper,” *J. Light. Technol.*, vol. 35, no. 11, pp. 2227–2233, 2017.
[6] R. Bustamante et al., “A compact and highly efficient SOI polarization splitter and rotator based on a bow-tie structure,” in *SBMO/IEEE MTT-S International Microwave and Optoelectronics Conference (IMOC)*, 2019, pp. 1–3.
[7] A. Xie, L. Zhou, J. Chen, and X. Li, “Efficient silicon polarization rotator based on mode-hybridization in a double-stair waveguide,” *Opt. Express*, vol. 23, no. 4, pp. 3960–3970, 2015.
[8] S. Kim and M. Qi, “Plasmonic mode-evolution-based polarization rotator and coupler,” in *2015 Conference on Lasers and Electro-Optics (CLEO)*, 2015, pp. 1–2.
[9] Z. Yu et al., “Subwavelength-structure-assisted ultracompact Polarization-handling Components on Silicon,” *J. Light. Technol.*, 2021.
[10]Z. Wang and D. Dai, “Ultrasmall Si-nanowire-based polarization rotator,” *JOSA B*, vol. 25, no. 5, pp. 747–753, 2008.